Development of a simplified numerical model for the design of 2G high-temperature superconductors

Kosheleva Natalia[1, 2], Shahrour Isam[1, *], Christian Eric Bruzek[3], Guillaume Vega[3] and Kolmogorov German[2]

[1]Laboratoire de Génie Civil et géo-Environnement
Université Lille1 – Science et Technologie
59650, Villeneuve d'Ascq, France
[2]Perm National Research Polytechnic University
29 Komsomolsky prospekt, Perm, Perm krai, Russia, 614990
[3]Nexans Reasech center Lens
92587, 4-10 rue Mozart, Clichy Cedex, France

ABSTRACT

Within the past few years robust superconductor known as Second-generation (2G) High Temperature Superconductor (HTS) were developed for different industrial applications. Their fabrication includes a phase of large bending, which induces both axial and shear stresses, which could lead to the degradation of the super-conductive substrate. The design of HTS requires analysis of the stress and strains induced during their fabrication. The use of the finite element method for the analysis of this complex material requires large meshes and computation time, because of the ultra-small thickness of the supra-conductive substrate. In this paper, we present a simplified model, which is based on the classical beam theory together with the discretization of each layer in small sub-layers working under purely axial stress. The model takes into consideration the plastic behaviour of the HTS constitutive materials. The model is validated by its confrontation to finite element analyses. Then it is used for the optimal design of HTS by the analysis of different industrial configurations. Analyses lead to some recommendations concerning the optimal configurations that reduce the stresses in the supra-conductive substrate.

Keywords: High-temperature superconductivity, Design, Mechanical numerical modeling, 2G HTS wire, Multilayer structure, YBCO, Plasticity, Finite element, Beam, Neutral axis

1. INTRODUCTION

Within the past few years robust superconductor known as Second-generation (2G) High Temperature Superconductor (HTS) were developed for different industrial applications, in particular for those in high energy density, nuclear, fusion and plasma applications. The superconducting tape is a multilayer structure composed of a metal substrate, a buffer layer, a superconducting layer and a stabilizing coating. For creating a chemical barrier between

*Corresponding Author: E-mail: isam.shahrour@univ-lille1.fr

the substrate and the HTS and matching their coefficients of thermal expansion (the difference in temperature between the application and the operating temperature can exceed 900°C), it is necessary to produce a buffer layer and to create a texture of HTS by its epitaxial growth. The layered internal structure of HTS in combination with extremely weak adhesion between their layers could lead to degradation of the HTS by delamination.

The fabrication of HTS encounters a major mechanical challenge concerning the degradation of the properties of conductors, due to the high mechanical stresses (Van der Laan & Ekin, 2008), (Van der Laan, et al., 2010). Experimental studies of the delamination process of HTS conductors 2nd generation were conducted by (Van der Laan, et al., 2007) and (Gorospe, et al., 2014). Researches on this issue were also conducted by (Jeong, et al., 2012), (Zhang, et al., 2011), (Myazato, et al., 2011), (Nishijima & Kitaguchi, 2012) and (Yanagisawa, et al., 2011), (Van der Laan, et al., 2007) and (Jeong, et al., 2012) showed that it was necessary to investigate the mechanicals properties of HTS materials in order to overcome the mechanical fragility problem. In some applications, the YBCO tape is submitted to bending. It is known that ceramic HTS tapes, which transmit power, could lose their conduction property by mechanical degradation during bending. Consequently, the analysis of the fabrication of HTS constitutes a challenging issue. It is expected from this analysis to determine the stresses and strains induced in the different layers of the HTS in taking into account the non-linear behavior of the different layers. The use of the finite element method for this analysis encounters major difficulty, because of the extra small thickness of some layers. This analysis required large meshes and computation time.

In this paper, we propose a simplified model for HTS material. This model is based on the beam theory together with the discretization of each layer in small sub-layers submitted working under purely axial stress. After the presentation of this model, we present its validation by its confrontation to finite element analyses and finally we use this model for the optimal design of HTS.

2. NUMERICAL MODEL

The model is based on the bending theory of beams. The beam section is composed of n layers. Each layer (i) is characterized by the thickness h_i, Young's Modulus E_i and axial stress strength ($\bar{\sigma}_l$). Each layer is subdivided in small sub-layers as illustrated in Figure 1. Each sub-layer is supposed to be submitted to purely axial stress σ_i.

We assume that the beam section is submitted to purely bending moment M (the axial force $N = 0$). The bending moment induces a rotation of the section around the neutral axis of the beam.

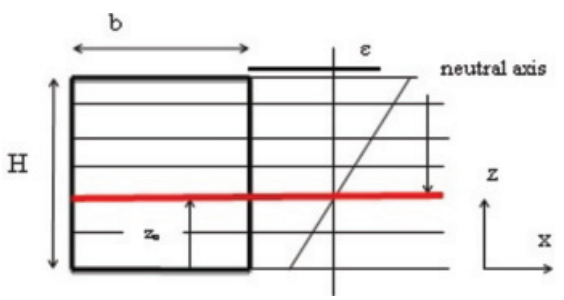

Figure 1: Configuration of the HTS beam section

2.1. ANALYSIS IN THE ELASTIC AREA

2.1.1. Axial stress distribution

The section is supposed to be submitted to the curvature (k), which induces the following strain in the section:

$$\varepsilon_i = k\left(z_i - z_n\right), \tag{1}$$

where z_n - is the position of the neutral axis, z_i - is the position of the i-th layer

The corresponding axial stress and force are equal to:

$$\sigma_i = \varepsilon_i E_i, \tag{2}$$

$$F_i = \sigma_i A_i, \tag{3}$$

where A_i is the cross-sectional area of i-th layer.

The location of neutral axis position (z_n) can be obtained using the equilibrium equation in the axial direction:

$$F = \sum_{i=1}^{n} F_i = k\sum_{i=1}^{n} A_i E_i (z_i - z_n) = 0, \tag{4}$$

which leads to the following expression:

$$z_n = \frac{\sum_{i=1}^{n} A_i E_i z_i}{\sum_{i=1}^{n} A_i E_i}, \tag{5}$$

The bending moment is given by:

$$M = \sum_{i=1}^{n} F_i (z_i - z_n) = \sum_{i=1}^{n} E_i k A_i (z_i - z_n)^2, \tag{6}$$

Equation (6) gives an explicit relationship between the bending moment and the curvature.

2.1.2. Shear stress distribution

The shear stress distribution is determined from the equilibrium of a small slide of the beam as illustrated in Figure 2. The slide is delimited by the lateral surfaces S_i and S_{i+1} and the lower surface B_i and the free up-surface. The lateral surfaces S_i and S_{i+1} are submitted to the axial force P_i and P_{i+1}, respectively, while the lower surface is submitted to the force $\tau_i\, dx$.

The equilibrium of the slide allows the determination of the shear stress as follows:

$$\tau_i = \frac{-P_{i+1} + P_i}{dx}, \tag{7}$$

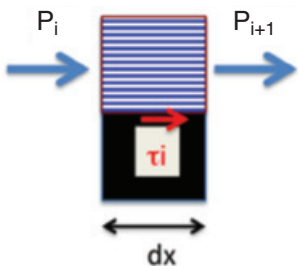

Figure 2: Determination of the shear stress

2.1.3. Beam deflection

According to the beam theory, the deflection (w) is determined by the integration of the following differential equation:

$$k(M) = \frac{d^2 w}{dx^2}, \tag{8}$$

2.2. PLASTIC AREA

2.2.1. Axial stress distribution

As in the elastic area, we assume that the rotation of the section around the natural axis induces the following strain:

$$\varepsilon_i = k\left(z_i - z_n\right), \tag{9}$$

The corresponding elastic axial stress is equal to:

$$\sigma_i = \varepsilon_i E_i, \tag{10}$$

This stress is submitted to the condition of plasticity:

$$\left|\sigma_i\right| \le \bar{\sigma}_i \tag{11}$$

With this condition the variation of the axial stress σ_i is not linear with the curvature k. It depends on the following parameters: k, z_n and $\bar{\sigma}_i$.

The corresponding axial force is equal to:

$$F_i = \sigma_i(k, z_n \text{ and } \bar{\sigma}_i) A_i, \tag{12}$$

The position of the natural axis (z_n) as well as k are determined from the resolution of the set of equations (4) to (6) and from (9) to (12). Since this set of equations is nonlinear, the resolution is conducted using an iterative procedure.

The bending moment is calculated according to the following equation:

$$M = \sum_{i=1}^{n} F_i (z_i - z_n), \tag{13}$$

Equation (13) gives the nonlinear relationship between the bending moment (M) and the curvature (k).

2.2.2. Shear stress distribution

The shear stress distribution is determined according from equation (7).

3. IMPLEMENTATION AND VALIDATION

3.1. IMPLEMENTATION IN MATLAB

The model presented in section 2 was implemented in MATLAB. The program, called (HTS_Analysis), uses a step-by-step analysis. At each step, we impose the curvature increment Δk. The values of the neutral axis (z_n), axial stress (σ) and axial stain (ε) are determined by the resolution of the nonlinear system of equations (4)–(6) and (9) to (12). The shear stress (τ) is computed from equation (7), while the corresponding bending moment is determined from equation (14). The program provides for the different values of the curvature (k) the corresponding values of the neutral axis (z_n), the axial stress (σ), the axial stain (ε), the shear stress (τ) and the bending moment (M).

3.2. VALIDATION

3.2.1. Presentation of the validation example

The program (HTS_Analysis) was checked by its confrontation to finite element analyses conducted by COMSOL Multiphysics software. Figure 3 shows the cantilever beam used in the analysis. Its length is equal to 300 µm, while its width is equal to 20 µm. The beam is composed of 4 layers. Table 1 summarizes the properties of these layers, which were taken from references (Clickner, et al., 2006) and (Osamura, et al., 2009).

The beam is submitted to an increasing uniform pressure at the upper surface (q).

3.2.2. Results

Figures 4 to 6 show a comparison between the results of COMSOL Multiphysics and those obtained by te simplified model (HTS_Analysis).

Figure 4 shows the distribution of the normal stress in the section $x = 35\ \mu m$ for two levels of the pressure $q = 300$ and $500\ N/m$. At $q = 300\ N/m$, we observe a linear variation of the normal stress in each layer. The stress remains in the elastic area. The results of the two

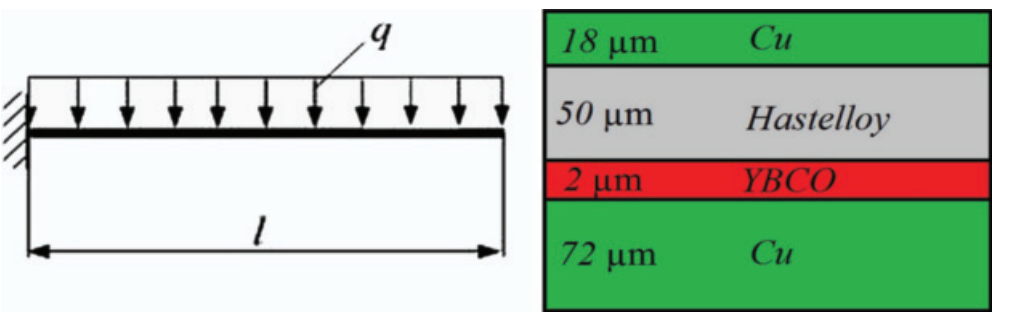

Figure 3: Beam used in the validation of the proposed model

Table 1: Properties of the beam used in the validation of the numerical model

Layer Number	**1**	**2**	**3**	**4**
Material	Cu	YBCO	Hastelloy	Cu
Height (µm)	72	2	50	18
Young's modulus (GPa)	110	128	192	110
Axial strength stress (MPa)	150	260	478	150

programs agree well. At q = 500 N/m, the two programs show a linear variation of the normal stress in the second and third layers and plasticity in the 1st and 4th layers.

Figure 5 shows the distribution of the shear stress in the section x = 35 μm for q = 300 and 500 N/m. At q = 300 N/m, the two programs show conventional variation of the shear

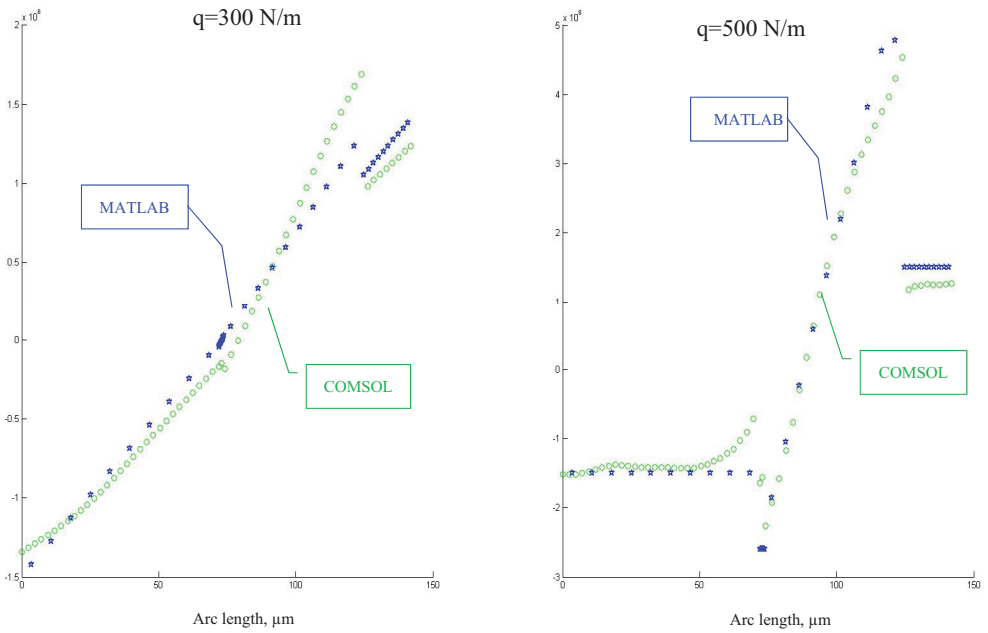

Figure 4: Validation of the simplified model (HTS_Analysis): Distribution of the normal stress in the section x = 35 μm at q = 300 and 500 N/m

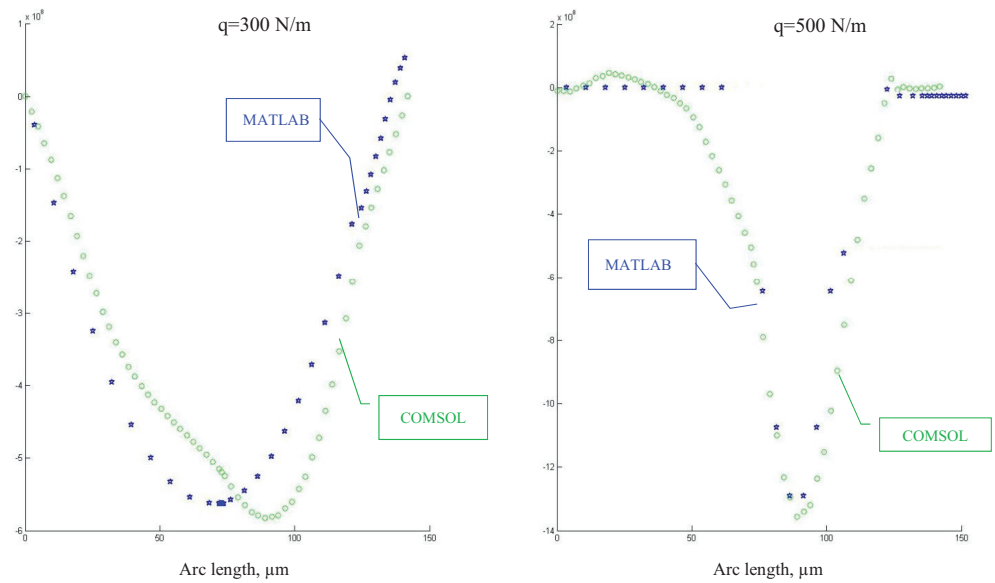

Figure 5: Validation of the simplified model (HTS_Analysis): Distribution of the shear stress in the section x = 35 μm at q = 300 and 500 N/m

stress in the beam section with a maximum near the beam axis, while at $q = 500\ N/m$, they show very low shear stresses in the zones close to the extremities of the beam (plastic area) and a concentration of the shear stress in the central part of the section.

Figure 6 shows the variation of the beam deflection in the section $x = 35\ \mu m$ with the increase in q. We observe a good agreement between COMSOL and HTS_Analysis. The deflection varies linearly with the pressure (q) up to $q = 300\ N/m$, then we observe a non-linear variation with an increase in the rate of deflection with the augmentation of the load. This increase results from the development of the plasticity in the beam.

This validation example shows that the simplified model globally well agrees with the results of the complex finite element analysis. It could be easily implemented in industrial environment and used in the HTS design.

4. APPLICATION TO THE OPTIMAL DESIGN OF HTS

In this section, the simplified model (HTS_Analysis) is used for the optimal design of HTS. The criteria used in this analysis concern the position of the neutral axis regarding the YBCO layer. The neutral axis during the process of bending should remain close to the YBCO layer in order to reduce the stresses in this fragile layer.

Analyses were conducted with three materials in the third layer: Hastelloy, NiW5 and Stainless steel, whose properties are summarized in table 2. The Young's modulus of Hastelloy and Stainless steel are close (around 192 *GPa*) and higher than that of NiW5 (111 *GPa*), while the axial strength of the stainless steel is about 62% of that of the Hastelloy and the axial strength of NiW5 is about 25% of that of Hastelloy.

For each material we have analyzed 4 cases, which correspond to different values of the thickness of the layers of the HTS proposed by the industry.

Table 3 summarizes the configurations analyzed with Hastelloy. The variation of the position of the neutral axis during bending is illustrated in Figure 7. We observe that in the first configuration (Case 1), the natural axis is faraway from the YBCO layer, while in

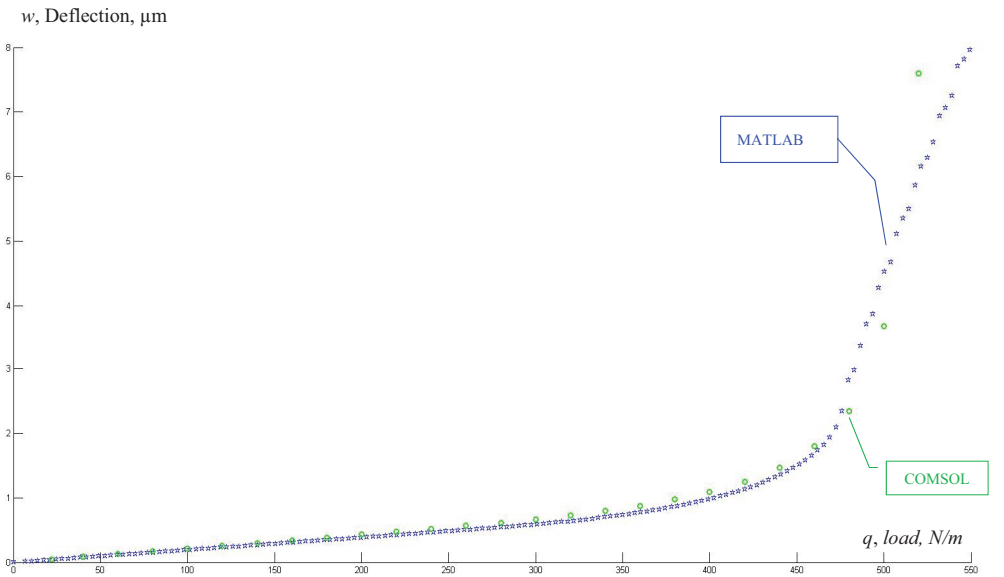

Figure 6: Validation of the simplified model (HTS_Analysis): Variation of the deflection in the section $x = 35\ \mu m$ with the load

Table 2: Mechanical properties of the materials used in the 3rd layer

	Young's modulus (GPa)	Axial strength stress (MPa)
Hastelloy	192	478
NiW5	111	121
Stainless steel	193	300

Table 3: Configurations analyzed with Hastelloy

Case (Layer)	1 (Cu)	2 (Cu)	3 (YBCO)	4 (Hastelloy)	5 (Cu)	Total Height (μm)
Case 1: height (μm)	18	52	2	50	18	140
Case 2: height (μm)	30	55	2	25	30	142
Case 3: height (μm)	18	45	2	25	18	108
Case 4: height (μm)	18	50	2	25	18	113

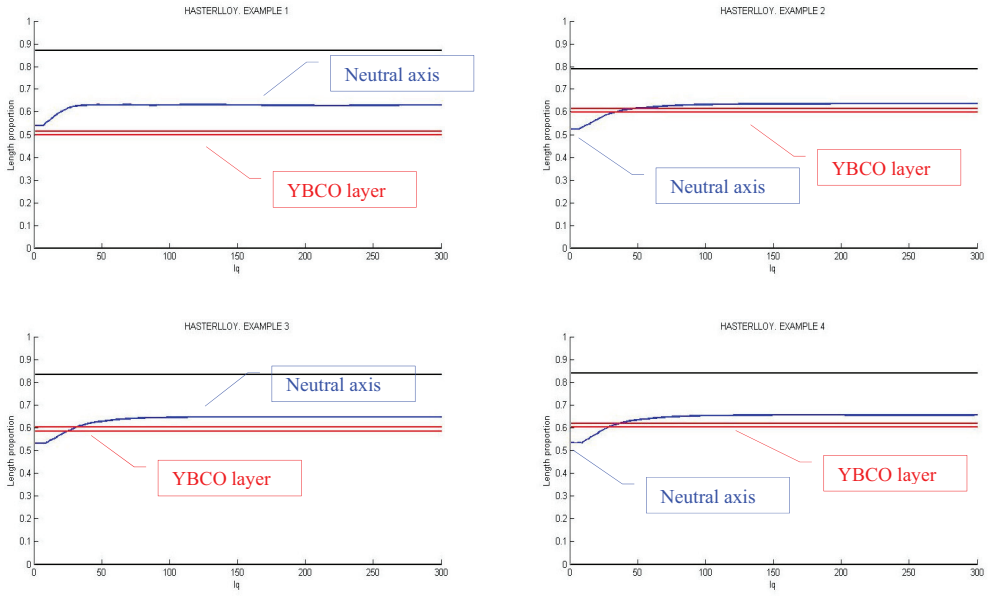

Figure 7: Variation of the position of the neutral axis during bending - HTS with Hastelloy layer; the characteristics of the 4 cases are summarized in table 3

the 3rd and 4th configurations, the neutral axis is below the YBCO layer in the elastic domain and then, it translates towards the upper surface and exceeds the YBCO layer by about 5% of the beam thickness. In the second configuration, the neutral axis is below the YBCO layer in the beginning of the loading and then it translates towards the upper part of the beam and stays close to the YBCO layer. This configuration is the best one, because the neutral axis remains close to the YBCO layer.

Table 4 summarizes the configurations analyzed with NiW5. The total thickness of the beam varies from 90 *μm* (Case 2) to 203 *μm* (Case 4); this large variation results from the large variation in the thickness of the 2nd and 4th layers.

Table 4: Configurations analyzed with NiW5

Case (Layer)	**1 (Cu)**	**2 (Cu)**	**3 (YBCO)**	**4 (NiW5)**	**5 (Cu)**	**Total Height (μm)**
Case 1: height (μm)	18	52	2	50	18	140
Case 2: height (μm)	18	27	2	25	18	90
Case 3: height (μm)	18	82	2	80	18	200
Case 4: height (μm)	18	90	2	75	18	203

The variation of the position of the neutral axis during bending is illustrated in Figure 8. We observe that in the configurations 1, 2 and 3, the neutral axis remains close to the YBCO layer, while in the 4th configuration; the neutral axis is below the YBCO layer by about 10% of the beam thickness. This configuration should not be used.

Table 5 summarizes the configurations analyzed with stainless steel. The total thickness of the beam varies from 108 μm (Case 3) to 142 μm (Case 2).

The variation of the position of the neutral axis during bending is illustrated in Figure 9. We observe that in the configurations 2, 3 and 4, the neutral axis remains close to the YBCO

Table 5: Configurations analyzed with stainless steel

Case (Layer)	**1 (Cu)**	**2 (Cu)**	**3 (YBCO)**	**4 (Stainless steel)**	**5 (Cu)**	**Total Height (μm)**
Case 1: height (μm)	18	52	2	50	18	140
Case 2: height (μm)	30	55	2	25	30	142
Case 3: height (μm)	18	45	2	25	18	108
Case 4: height (μm)	18	50	2	25	18	113

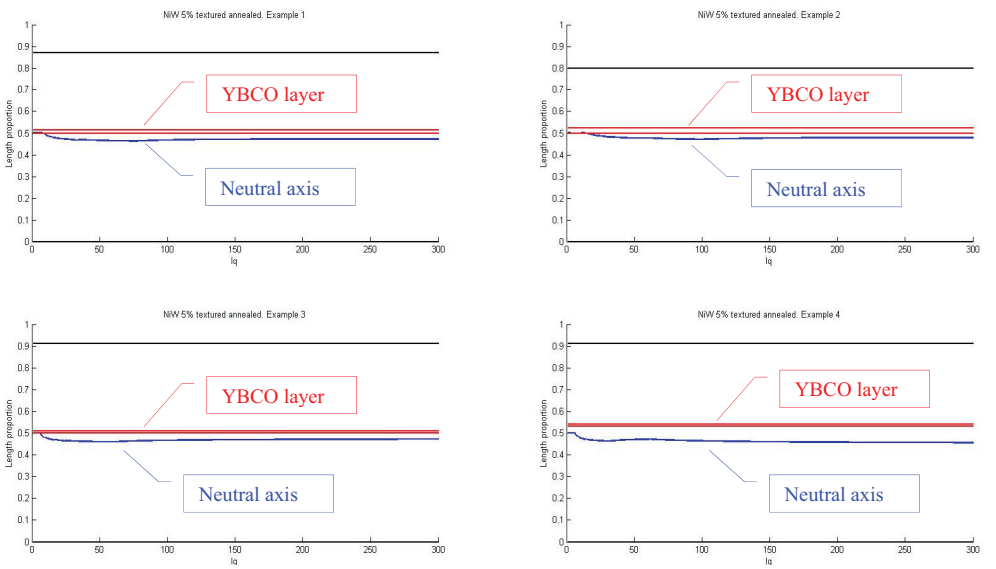

Figure 8: Variation of the position of the neutral axis during bending - HTS with NiW5 layer; the characteristics of the 4 cases are summarized in table 4

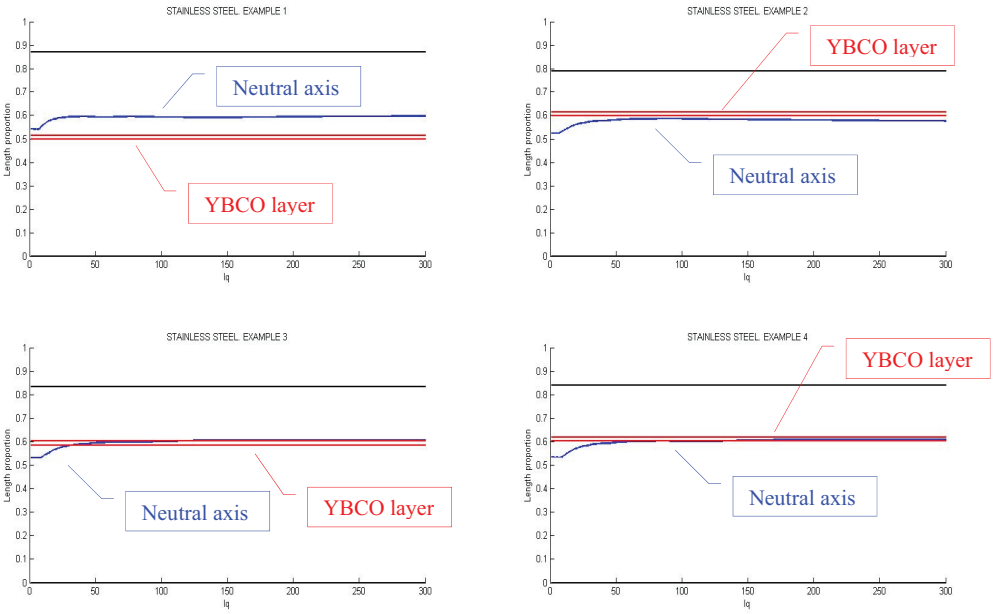

Figure 9: Variation of the position of the neutral axis during bending - HTS with stainless steel; the characteristics of the 4 cases are summarized in table 5

layer in the plastic area, while in the 1st configuration, the neutral axis is above the YBCO layer by about 10% of the beam thickness. This configuration is then not recommended.

5. CONCLUSION

The fabrication of 2G high-temperature superconductors (HTS) includes a phase of large bending, which induces both axial and shear stresses in the HTS. The optimal design requires keeping the neutral axis close to the supra-conductive substrate. The use of finite element method for the analysis of this complex material requires large meshes and computation time, because of the ultra-small thickness of the supra-conductive substrate. In this paper, we presented a simplified model, which is based on the classical beam theory together with the discretization of each layer in small sub-layers working under purely axial stresses. The model takes into consideration the plastic behavior of the HTS constitutive materials. The model was validated by its confrontation to finite element analyses. The validation test gave satisfactory results. This model could be easily implemented and used in industrial environment.

The model was used for the optimal design of HTS by the analysis of different industrial configurations. Analysis resulted in recommendations for the optimal configurations that reducing stresses in the supra-conductive substrate.

REFERENCES

[1] Gorospe, A., Nisay, A. and Shin, H.-S., 2014. Delamination behaviour in differently copper laminated REBCO coated conductor tapes under transverse loading. *Physica C*, Volume 504, pp. 47–52.

[2] Jeong, H., Park, H., Kim, S. et al., 2012. Delamination characteristics of coated conductor for conduction cooled HTS coil. *IEEE Transaction on applied superconductivity*, 22(3).

[3] Myazato, T., Hojo, M. et al., 2011. Mode I type delamination fracture toughness of YBCO coated conductor with additional Cu layer. *Physica C*, Volume 471, pp. 1071–1074.

[4] Nishijima, G. and Kitaguchi, H., 2012. Transport and mechanical property evaluation for Cu stabilized PLD-GdBa CuO coated conductor. *IEEE Transactions on applied superconductivity*, 22(3).

[5] Van der Laan, D. C., Eckin, J. W., Clickner, C. C. and Stauffer, T. C., 2007. Delamination strength of YBCO coated conductors under transverse tensile stress. *Superconductor Science and Technology*, Issue 20, pp. 765–770.

[6] Van der Laan, D. C. and Ekin, J. W., 2008. Dependence of the critical current of YBa2Cu3O7–δ coated conductors on in-plane bending. *Superconductor Science and Technology*, Issue 21, pp. 1–6.

[7] Van der Laan, D. C. et al., 2010. Effect of strain, magnetic field and field angle on the critical current density of YBa2Cu3O7–δ coated conductors. *Superconductor Science and Technology*, Issue 23, pp. 1–7.

[8] Yanagisawa, Y., Nakagome, H., Nakagome, H. et al., 2011. Remarkable weakness against cleavage stress for YBCO-coated conductors and its effect on the YBCO coil performance. *Physica C*, Volume 471, pp. 480–485.

[9] Zhang, Y., Duvall, J., Knoll, A. et al., 2011. *Development of testing method for adhesion strength characteriza-tion of 2G HTS wire*. Osaka, The 15th Japan – US Workshop on Advanced Superconductors.